Compensation-doped silicon for photovoltaic applications

Georgy Samsonidze, Marvin L. Cohen, and Steven G. Louie

Phys. Rev. B **84**, 195201 — Published 4 November 2011

DOI: 10.1103/PhysRevB.84.195201

Compensation-doped silicon for photovoltaic applications

Georgy Samsonidze, Marvin L. Cohen, and Steven G. Louie
Department of Physics, University of California, Berkeley, CA 94720, USA and
Materials Sciences Division, Lawrence Berkeley National Laboratory, Berkeley, CA 94720, USA
(Dated: September 14, 2011)

A small overlap between the silicon optical absorption spectrum and the solar spectral irradiance limits the conversion efficiency of crystalline thin-film silicon solar cells. In this work, a theoretical search for compensation-doped silicon is carried out aiming to maximize the spectral overlap. First, a wide range of dopant species and concentrations is considered using the virtual crystal approximation and the empirical pseudopotential method. Second, the most promising modifications of silicon are investigated using the supercell method and a first-principles many-electron Green's function approach. In both steps, the optical absorption spectrum is computed by solving the Bethe-Salpeter equation to include excitonic effects. It is found that the conversion efficiency of a silicon film of 10 μm thickness can be increased by 25 % by a 1.6 at. % compensation doping with In and Sb.

I. INTRODUCTION

The energy conversion efficiency of a single junction solar cell is mostly limited by (1) the loss of photons with energy below the band gap and (2) the thermalization of photoexcited electrons and holes to the band edges[1,2]. The conversion efficiency reaches the maximum value of 45 % (33 % including contributions from other less-efficient loss mechanisms) for an optimal band gap of 1.31 eV[2]. The indirect band gap of silicon $E_g = 1.12$ eV measured at room temperature[3] is not too far from the optimal value. This is one of the prerequisites that led to the success of crystalline silicon technology on the photovoltaic (PV) market[4]. There is also a growing interest in thin-film silicon technology because of the high costs of silicon wafers[5,6]. However, the conversion efficiency of thin-film silicon solar cells is somewhat limited by their relatively small optical absorption in the visible range. The direct band gap of silicon is $E_g' = 3.32$ eV at room temperature[7] which results in a low probability for the absorption process in the range of photon energies between E_g and E_g'.

In this paper, a theoretical search for substitutionally doped silicon is conducted with the goal to maximize the overlap between the optical absorption spectrum and the solar spectral irradiance. We consider compensation doping (equal amounts of donor and acceptor impurity species) to avoid introducing free charge carriers. As a first step, different dopant species at various concentrations are examined using the virtual crystal approximation[8] and the empirical pseudopotential method[9]. The virtual crystal approximation allows us to probe a wide range of dopant concentrations, and the empirical pseudopotential method makes it easy to consider many different dopant species at low computational cost. For each dopant species and concentration the optical absorption spectrum of the modified silicon is computed by solving the Bethe-Salpether equation (BSE) which describes the Coulomb correlation between the photoexcited electron and hole[10,11]. The conversion efficiency is estimated using the reference solar spectral irradiance[12] and including "below the band gap" and "thermalization" losses[1,2]. Several most promising modifications of silicon identified through this process are further investigated using the supercell method[13] and a first-principles many-electron Green's function approach (the GW-BSE approach)[10,11,14,15].

This paper is organized as follows. In Section II, the conversion efficiency of thin-film silicon is examined. In Section III, the effect of different dopant species and concentrations on the conversion efficiency is estimated. In Section IV, the best identified modifications of silicon are further investigated using more accurate methodology. The key results are summarized in Section V.

II. CONVERSION EFFICIENCY

The two necessary components for evaluating the energy conversion efficiency of a solar cell are the solar spectral irradiance $I(\omega)$ and the imaginary part of the dielectric function $\epsilon_2(\omega)$ of the material where ω is the photon angular frequency. We employ the reference $I(\omega)$ at sea level (so called "global tilt")[12] and we compile $\epsilon_2(\omega)$ of silicon from three different experiments: infrared transmission spectroscopy for $\hbar\omega < 1.4$ eV[16], ellipsometry for 1.7 eV $< \hbar\omega <$ 5.7 eV[7], and reflectance spectroscopy for $\hbar\omega > 5$ eV[17] where $\hbar$ is Planck constant. Both $I(\omega)$ and $\epsilon_2(\omega)$ are shown in Fig. 1(a) as a function of ω. The real part of the dielectric function $\epsilon_1(\omega)$ can be obtained from $\epsilon_2(\omega)$ using the Kramers-Kronig relations[18]. The refractive index $n(\omega)$ and the extinction coefficient $\kappa(\omega)$ are then computed according to the following relation:

$$n(\omega) + i\kappa(\omega) = \sqrt{\epsilon_1(\omega) + i\epsilon_2(\omega)}. \tag{1}$$

The absorption coefficient is given by:

$$\alpha(\omega) = \frac{2\omega}{c}\kappa(\omega). \tag{2}$$

The incident irradiance is obtained by integrating $I(\omega)$ over the photon energy spectrum:

$$I_i = \int_0^\infty I(\omega)\, d\omega. \tag{3}$$

Only part of it will be absorbed because of the loss of photons with energy below the band gap and the finite thickness of the silicon film. Both of these factors are reflected in the equation for the absorbed irradiance:

$$I_a(L) = \int_{E_g/\hbar}^\infty \left[1 - e^{-\alpha(\omega)L}\right] I(\omega)\, d\omega \tag{4}$$

where L is the thickness of the silicon film. The photoexcited electrons and holes rapidly thermalize to the band edges so that the part of the photon energy above the band gap is lost to heat. This loss is accounted for by introducing an additional factor of $E_g/(\hbar\omega)$ in Eq. (4). We thus arrive at the following expression for the delivered irradiance:

$$I_d(L) = \int_{E_g/\hbar}^{\infty} \left[1 - e^{-\alpha(\omega)L}\right] I(\omega) \frac{E_g}{\hbar\omega} \, d\omega. \tag{5}$$

The conversion efficiency is defined as follows:

$$\eta(L) = \frac{I_d(L)}{I_i}. \tag{6}$$

We plot I_i, $I_a(L)$ and $I_d(L)$ in Fig. 1(b) as a function of L. The asymptotes of $I_a(L)$ and $I_d(L)$ in the limit of bulk silicon ($L \to \infty$) are shown by the dashed lines. The vertical difference between the I_i and $I_a(L)$ curves represents "below the band gap" loss and the difference between $I_a(L)$ and $I_d(L)$ is "thermalization" loss. For $L \to \infty$ we find that "below the band gap" loss is 19 %, "thermalization" loss is 32 %, and $\eta(\infty) = 49$ %; this is similar to the values reported in the literature for a device with $E_g = 1.31$ eV: 25 %, 30 % and 45 %, respectively[2].

III. SCANNING OF DOPANTS

Let us proceed with computing $\epsilon_2(\omega)$ for compensation-doped silicon films. Our goal in this section is to scan a large number of dopant species and to identify the ones that maximize the conversion efficiency defined by Eq. (6). We choose the empirical pseudopotential method (EPM) for its simplicity and low computational cost, yet accurate description of the band structure of zinc-blende semiconductors[9], and we employ the TBPW code[19]. The EPM band structure and wave functions are used as input for the Bethe-Salpether equation (BSE) which describes the Coulomb correlation between photoexcited electron and hole or the excitonic effects[10,11]. Upon solving the BSE, the excitonic energy and wave functions are used to compute $\epsilon_2(\omega)$ following the approach of Rohlfing and Louie[11]. This does not include the indirect absorption contribution to $\epsilon_2(\omega)$ which arises from phonon-assisted interband transitions. We add to the calculated $\epsilon_2(\omega)$ the contribution from indirect absorption processes which takes the following form[20]:

$$\epsilon_2(\omega) = C m_e^{3/2} m_h^{3/2} (\hbar\omega - E_g)^2 \tag{7}$$

where $m_e = 1.06$ and $m_h = 0.87$ are the density-of-states effective masses for electrons and holes near the band edges in units of free electron mass and C is the coefficient proportional to the squared absolute values of electron-photon and electron-phonon matrix elements. We find $C = 0.16$ eV^{-2} by fitting Eq. (7) to infrared transmission spectroscopy data[16]. The computed $\epsilon_2(\omega)$ for pure silicon is shown in Fig. 2(a) where the experimental $\epsilon_2(\omega)$ is plotted using a dashed line for comparison.

Within the EPM, the electronic structure of silicon is determined by four parameters: the lattice constant $a = 5.43$ Å and three symmetric potential form factors, $V_3^S = -0.224$ Ry, $V_8^S = 0.055$ Ry and $V_{11}^S = 0.072$ Ry[9,21] where the subscript G^2 is the square of the length of the reciprocal lattice vector in units of $2\pi/a$. There are also three antisymmetric form factors V_3^A, V_4^A and V_{11}^A which are zero for elemental compounds in the diamond structure but are not zero for binary compounds[9].

To sample every possible modification of silicon, each of the seven EPM parameters is varied around its value for silicon and $\epsilon_2(\omega)$ is calculated. Also, the indirect transitions' contribution to $\epsilon_2(\omega)$ is evaluated using the resulting EPM effective masses and band gaps in Eq. (7). The conversion efficiency of the modified silicon film of thickness $L = 100$ nm, $\eta_m(L)$, is then computed according to Eqs. (1)–(6). The ratio of $\eta_m(L)$ to the conversion efficiency of the pure silicon film of the same thickness $L = 100$ nm, $\eta_0(L)$, is shown in Figs. 2(b)–(d) as a function of variation in each of the seven EPM parameters. The range of variation of the EPM parameters roughly corresponds to that of 0 to 4 at. % doping as follows from the virtual crystal model given below. Based on the results shown in Figs. 2(b)–(d), the conversion efficiency is maximized by increasing a, decreasing V_8^S and V_{11}^S and varying V_4^A.

We attempt to use these rough predictions to examine real material candidates. The EPM parameters for 15 different semiconductors in addition to silicon—group VI elemental compounds and group III-V and II-VI binary compounds—are available in the literature[9,21]. The virtual crystal approximation is employed to construct the EPM parameters for silicon doped with these compounds at the level of 4 at. % which is representative for the variation of the EPM parameters shown in Figs. 2(b)–(d). First, the symmetric and antisymmetric form factors are converted to the atomic form factors[9]:

$$\begin{cases} V_{G^2}^1 = V_{G^2}^S + V_{G^2}^A, \\ V_{G^2}^2 = V_{G^2}^S - V_{G^2}^A. \end{cases} \tag{8}$$

Second, one of the two functional forms of the atomic potential is fitted to the atomic form factors[22]:

$$V_{\pm}(q) = \frac{C_1\left(q^2 - C_2\right)}{\exp\left(C_3\left(q^2 + C_4\right)\right) \pm 1} \tag{9}$$

where $q = 2\pi G/a$ is the reciprocal lattice vector. We use $V_{-}(q)$ and $V_{+}(q)$ for the elemental and binary compounds, respectively. Third, the lattice constant of the modified silicon (a_m) is computed from the lattice constants of the pure silicon (a_0) and the doping compound (a_d) using the condition that the crystal volume is kept constant:

$$a_m = \sqrt[3]{(1-x)\, a_0^3 + x a_d^3} \tag{10}$$

where $x = 0.04$ is the doping level. Fourth, the new atomic form factors are computed from the fitted atomic potentials $V_{\pm}(q)$ at the new values of the reciprocal lattice vectors (since $q \propto a^{-1}$). Fifth, the atomic form factors of the pure silicon and the doping compound are mixed:

$$V^{1,2}_{G^2 m} = (1-x)\, V^{1,2}_{G^2 0} + x V^{1,2}_{G^2 d}. \tag{11}$$

Sixth, the atomic form factors are converted to the symmetric and antisymmetric form factors[9]:

$$\begin{cases} V^{S}_{G^2 m} = \dfrac{1}{2}\left(V^{1}_{G^2 m} + V^{2}_{G^2 m}\right), \\ V^{A}_{G^2 m} = \dfrac{1}{2}\left(V^{1}_{G^2 m} - V^{2}_{G^2 m}\right). \end{cases} \tag{12}$$

Using the lattice constant and the form factors of the modified silicon given by Eqs. (10) and (12), respectively, the conversion efficiency $\eta_m(L)$ at $L = 100$ nm is obtained from the curves plotted in Figs. 2(b)–(d). The ratios $\eta_m(L)/\eta_0(L)$ for different dopant species at the doping level of 4 at. % are summarized in Table I. According to Table I, the conversion efficiency at $L = 100$ nm is increased by 12 % upon compensation doping with In and Sb and by 9 % upon doping with Sn. Note that the conversion efficiency within each of the three classes of dopant species—group VI, III-V and II-VI compounds—increases with decreasing the band gap of the doping compound, with the only exception of AlSb. Indeed, within the virtual crystal approximation, the change in the band gap of the modified silicon is proportional to the band gap of the doping compound. For a thin silicon film ($L = 100$ nm), decreasing the band gap increases the conversion efficiency because "below the band gap" loss far exceeds "thermalization" loss as seen in Fig. 1(b).

IV. BEST CANDIDATES

The predictions of Section III are now verified using more accurate *ab initio* methodology. In what follows, $\epsilon_2(\omega)$ of bulk silicon and silicon supercells with substitutional impurity atoms is computed from first-principles. First, the density-functional theory (DFT) calculation is carried out for bulk silicon employing the plane-wave pseudopotential code PARATEC[23] and using norm-conserving pseudopotentials[24] in nonlocal separable form[25], the local density approximation (LDA)[26] for the exchange-correlation potential, 32 Ry kinetic energy cutoff for the plane-wave expansion of wave-functions, and a $4 \times 4 \times 4$ shifted Monkhorst-Pack grid of $\mathbf{k}$ points in reciprocal space (k-grid)[27]. Second, the quasiparticle energies are calculated within the G_0W_0 approximation[14,15] employing the Berkeley GW package[28] and using 10 Ry kinetic energy cutoff for the plane-wave expansion of the dielectric function and 133 unoccupied bands with eigenvalues up to 10 Ry above the averaged DFT potential. Third, the BSE equation is solved and $\epsilon_2(\omega)$ is computed with BerkeleyGW[28]. The electron-hole interaction kernel for 4 occupied and 10 unoccupied bands is evaluated on a $4 \times 4 \times 4$ unshifted coarse k-grid and extrapolated to a $10 \times 10 \times 10$ shifted fine k-grid. Fourth, the indirect absorption edge given by Eq. (7) is added to $\epsilon_2(\omega)$. The resulting $\epsilon_2(\omega)$ (solid line) is shown in Fig. 3(a) where the experimental $\epsilon_2(\omega)$ is plotted (dashed line) for comparison.

Next, silicon supercells including the substitutional impurity atoms are constructed. They are built from the conventional unit cell Si_8 which consists of four primitive unit cells Si_2. For doping with group IV elements, Si_{64} supercell of $2 \times 2 \times 2$ conventional unit cells is used. For compensation doping with group III and V elements, Si_{128} supercell of $4 \times 2 \times 2$ conventional unit cells is used. In the case of Si_{128} supercell, the electrostatic interactions are minimized by choosing the lattice vectors as follows: $\mathbf{a}_1 = (4a, 0, 0)$, $\mathbf{a}_2 = (2a, 2a, 0)$ and $\mathbf{a}_3 = (2a, 0, 2a)$. This ensures that each group III impurity has group V impurities as its nearest neighbors, and vice versa. Introducing one impurity atom in Si_{64} supercell or two impurity atoms in Si_{128} supercell corresponds to a doping level of 1.6 at. %. Doping with elements In, Sb and Sn is considered based on the results of Section III. Also, B, Al and Ge are

examined because these impurities are common in the silicon industry and because there are no EPM parameters available for B. The following supercells are constructed: Si_{64}, $Si_{63}Ge$, $Si_{63}Sn$, Si_{128}, $Si_{126}BP$, $Si_{126}BAs$, $Si_{126}AlSb$ and $Si_{126}InSb$, and the atomic positions are optimized using the DFT forces and stresses. The kinetic energy cutoffs for wave-functions are chosen according to the hardest pseudopotential impurity atom, and $2 \times 2 \times 2$ and $1 \times 2 \times 2$ shifted k-grids are used for 64- and 128-atom supercells, respectively. The GW calculations are carried out using 5 Ry kinetic energy cutoff for the dielectric function and 1447 and 2887 unoccupied bands with eigenvalues up to 5 Ry above the averaged DFT potential for 64- and 128-atom supercells, respectively. The BSE calculations are conducted employing 36 occupied and 32 unoccupied bands that span the energy range of 2 eV above the band edges for 64-atom supercells, and 52 occupied and 64 unoccupied bands also in the energy range of 2 eV for 128-atom supercells. The electron-hole interaction kernel is evaluated at the Γ-point and extrapolated to $4 \times 4 \times 4$ and $2 \times 4 \times 4$ shifted fine k-grids for 64- and 128-atom supercells, respectively. For the indirect absorption edge of Eq. (7), the effective masses for electrons and holes are computed within DFT and the band gaps within GW. The resulting $\epsilon_2(\omega)$ for 64- and 128-atom supercells are shown in Figs. 3(b) and (c), respectively. Note that these have smaller magnitudes at high frequencies ($\hbar\omega > 3$ eV) compared to the one plotted in Fig. 3(a). This is because only the bands in a 2 eV energy window above the fundamental band gap ($E_g = 1.12$ eV) are included in the BSE due to a high computational cost. However, for our purposes we are only interested in the low-frequency side of $\epsilon_2(\omega)$ and it turns out to be converged with the bands in a 2 eV window above E_g.

For each supercell, the conversion efficiency $\eta_m(L)$ for film thicknesses $L = 100$ nm, $L = 1$ μm and $L = 10$ μm is computed according to Eqs. (1)–(6) using $\epsilon_2(\omega)$ from Figs. 3(b) and (c). The ratios of $\eta_m(L)$ to the conversion efficiencies $\eta_0(L)$ of pure silicon films of the same thicknesses are listed in Table II. The results summarized in Table II are in qualitative agreement with the rough predictions of Section III. Namely, it is found that the conversion efficiency of silicon films is maximized by compensation doping with In and Sb or by doping with Sn. However, the increase in the conversion efficiency is considerably larger than predicted in Section III. There can be several reasons for why this increase is not captured within the EPM/BSE framework of Section III including the absence of the local lattice distortion around the defect sites, the undisturbed periodicity imposed by the virtual crystal approximation and the approximate nature of the empirical pseudopotential method. Further calculations such as the DFT/GW-BSE in the virtual crystal approximation, the DFT/GW-BSE for the unrelaxed supercell, the EPM/BSE for the unrelaxed supercell and the EPM/BSE for the supercell relaxed with DFT will be required if one wishes to identify the relative influence of the aforementioned factors. It is important to note that the increase in $\eta_m(L)/\eta_0(L)$ drops with increasing L as one can see from Table II. For small L, the increase in $\eta_m(L)/\eta_0(L)$ is caused by the red-shift of the low-frequency side of $\epsilon_2(\omega)$ in Figs. 3(b) and (c). As L increases, however, $\eta_0(L)$ approaches $\eta_m(L)$ because indirect transitions dominate the absorption. It is found that for $L = 10$ μm, the conversion efficiency can be increased by 25 % by a 1.6 at. % compensation doping with In and Sb.

V. SUMMARY

In this paper, we attempt to maximize the overlap between the optical absorption spectrum of modified silicon films and the solar spectral irradiance by compensation doping. For evaluating the conversion efficiency of silicon, the two most important intrinsic loss mechanisms are considered, and the less important other intrinsic and all extrinsic losses are ignored. First, different dopant species are examined using the virtual crystal approximation and the empirical pseudopotential method. Second, several most promising dopant species are investigated using the supercell method and a first-principles many-electron Green's function approach. It is found that the conversion efficiency of the silicon film of 10 μm thickness can be increased by 25 % by a 1.6 at. % compensation doping with In and Sb (0.8 at. % of In and 0.8 at. % of Sb). This is somewhat larger than the solid solubility limits of In and Sb in silicon[29–31], but this is the lowest doping level that can be investigated easily from first-principles. We note also that the relative increase in the conversion efficiency induced by compensation doping decreases with increasing thickness of the silicon film because of indirect absorption processes. The effective optical thickness in actual devices can be increased using Lambertian light-trapping schemes[32].

ACKNOWLEDGMENTS

The work described in Section III was carried out using methods and codes developed with support from National Science Foundation Grant No. DMR10-1006184. Computational resources have been provided by NSF through TeraGrid resources at NICS. The work described in Section IV was carried out using methods and codes developed with support from the Director, Office of Science, Office of Basic Energy Sciences, Materials Sciences and Engineering

Division, U.S. Department of Energy under Contract No. DE-AC02-05CH11231. Computational resources have been provided by DOE at Lawrence Berkeley National Laboratory's NERSC facility.

[1] W. Shockley and H. J. Queisser, J. Appl. Phys. **32**, 510 (1961).
[2] L. C. Hirst and N. J. Ekins-Daukes, Prog. Photovolt: Res. Appl. **19**, 286 (2011).
[3] W. Bludau, A. Onton, and W. Heinke, J. Appl. Phys. **45**, 1846 (1974).
[4] R. G. Little and M. J. Nowlan, Prog. Photovolt: Res. Appl. **5**, 309 (1997).
[5] K. L. Chopra, P. D. Paulson, and V. Dutta, Prog. Photovolt: Res. Appl. **12**, 69 (2004).
[6] F. Duerinckx, K. V. Nieuwenhuysen, H. Kim, I. Kuzma-Filipek, H. Dekkers, G. Beaucarne, and J. Poortmans, Prog. Photovolt: Res. Appl. **13**, 673 (2005).
[7] P. Lautenschlager, M. Garriga, L. Vina, and M. Cardona, Phys. Rev. B **36**, 4821 (1987).
[8] R. J. Elliott, J. A. Krumhansl, and P. L. Leath, Rev. Mod. Phys. **46**, 465 (1974).
[9] M. L. Cohen and T. K. Bergstresser, Phys. Rev. **141**, 789 (1966).
[10] G. Strinati, Riv. Nuovo Cimento **11**, 1 (1988).
[11] M. Rohlfing and S. G. Louie, Phys. Rev. B **62**, 4927 (2000).
[12] ASTM Standard G173–03, 2008, "Standard Tables for Reference Solar Spectral Irradiances: Direct Normal and Hemispherical on 37° Tilted Surface," ASTM International, West Conshohocken, PA, 2008, DOI: 10.1520/G0173-03R08, `www.astm.org`.
[13] M. L. Cohen, M. Schlüter, J. R. Chelikowsky, and S. G. Louie, Phys. Rev. B **12**, 5575 (1975).
[14] L. Hedin and S. Lundqvist, in *Advances in Research and Applications*, Solid State Physics, Vol. 23, edited by F. Seiz, D. Turnbull, and H. Ehrenreich (Academic Press, 1970) pp. 1 – 181.
[15] M. S. Hybertsen and S. G. Louie, Phys. Rev. B **34**, 5390 (1986).
[16] G. G. Macfarlane and V. Roberts, Phys. Rev. **98**, 1865 (1955).
[17] H. R. Philipp, J. Appl. Phys. **43**, 2835 (1972).
[18] J. S. Toll, Phys. Rev. **104**, 1760 (1956).
[19] R. M. Martin, *Electronic Structure: Basic Theory and Practical Methods* (Cambridge University Press, 2004).
[20] P. Y. Yu and M. Cardona, *Fundamentals of Semiconductors*, 4th Revised edition (Springer-Verlag Berlin and Heidelberg GmbH & Co. K, 2010).
[21] Damocles Web Site, 1999, IBM Research, `http://www.research.ibm.com/DAMOCLES/home.html`.
[22] S. B. Zhang, C.-Y. Yeh, and A. Zunger, Phys. Rev. B **48**, 11204 (1993).
[23] B. G. Pfrommer, J. Demmel, and H. Simon, J. Comp. Phys. **150**, 287 (1999).
[24] N. Troullier and J. L. Martins, Phys. Rev. B **43**, 1993 (1991).
[25] L. Kleinman and D. M. Bylander, Phys. Rev. Lett. **48**, 1425 (1982).
[26] J. P. Perdew and A. Zunger, Phys. Rev. B **23**, 5048 (1981).
[27] H. J. Monkhorst and J. D. Pack, Phys. Rev. B **13**, 5188 (1976).
[28] J. Deslippe, G. Samsonidze, D. Strubbe, M. Jain, M. L. Cohen, and S. G. Louie, Comput. Phys. Comm. (to be published).
[29] J. D. Plummer, M. D. Deal, and P. B. Griffin, *Silicon VLSI Technology: Fundamentals, Practice, and Modeling*, 2nd edition (Prentice Hall Press, Upper Saddle River, 2008).
[30] F. A. Trumbore, Bell System Tech. Journal **39**, 205 (1960).
[31] J. D. Plummer and P. B. Griffin, Proc. IEEE **89**, 240 (2001).
[32] M. A. Green, in *Clean Electricity from Photovoltaics*, Series on Photoconversion of Solar Energy, Vol. 1, edited by M. D. Archer and R. Hill (Imperial College Press, London, 2001).

TABLE I. Ratio of the conversion efficiency of the modified silicon $\eta_m(L)$ to that of pure silicon $\eta_0(L)$ for different dopant species computed in the virtual crystal approximation within the EPM/BSE approach of Sec. III. The compensation doping level is 4 at. % and the thickness of the silicon film is $L = 100$ nm.

$\eta_m(L)/\eta_0(L)$	100 nm
$Si_{0.96}Ge_{0.04}$	1.035
$Si_{0.96}Sn_{0.04}$	1.093
$Si_{0.96}Al_{0.02}P_{0.02}$	1.019
$Si_{0.96}Al_{0.02}As_{0.02}$	1.026
$Si_{0.96}Al_{0.02}Sb_{0.02}$	1.071
$Si_{0.96}Ga_{0.02}P_{0.02}$	1.032
$Si_{0.96}Ga_{0.02}As_{0.02}$	1.048
$Si_{0.96}Ga_{0.02}Sb_{0.02}$	1.058
$Si_{0.96}In_{0.02}P_{0.02}$	1.044
$Si_{0.96}In_{0.02}As_{0.02}$	1.059
$Si_{0.96}In_{0.02}Sb_{0.02}$	1.116
$Si_{0.96}Zn_{0.02}S_{0.02}$	1.059
$Si_{0.96}Zn_{0.02}Se_{0.02}$	1.062
$Si_{0.96}Zn_{0.02}Te_{0.02}$	1.069
$Si_{0.96}Cd_{0.02}Te_{0.02}$	1.084

TABLE II. Ratio of the conversion efficiency of the modified silicon $\eta_m(L)$ to that of pure silicon $\eta_0(L)$ for different dopant species computed using the supercell method within the DFT/GW-BSE approach of Sec. IV. The compensation doping level is 1.6 at. % and the thickness of the silicon film is $L = 100$ nm, 1 μm and 10 μm.

$\eta_m(L)/\eta_0(L)$	100 nm	1 μm	10 μm
$Si_{63}Ge$	1.180	1.031	1.017
$Si_{63}Sn$	1.385	1.098	1.083
$Si_{126}BP$	1.202	1.116	1.026
$Si_{126}BAs$	1.350	1.317	1.094
$Si_{126}AlSb$	1.293	1.198	1.053
$Si_{126}InSb$	1.524	1.448	1.248

FIG. 1. (a) Reference solar spectral irradiance[12] and imaginary part of the dielectric function of silicon measured experimentally as a function of the photon energy[7,16,17]. The vertical lines indicate the indirect and direct band gaps of silicon[3,7]. The inset shows the indirect absorption region on an expanded scale. (b) Incident, absorbed and delivered irradiance as a function of silicon film thickness computed from Eqs. (3)–(5). The dashed lines show the absorbed and delivered irradiance in the limit of bulk silicon.

FIG. 2. (a) Imaginary part of the dielectric function of silicon computed within the EPM/BSE approach of Sec. III, including the indirect absorption edge as given by Eq. (7). The dashed line shows the experimental dielectric function from Fig. 1(a). The inset shows the indirect absorption region near $\hbar\omega = 2$ eV. (b)–(d) Ratio of the conversion efficiency of the modified silicon $\eta_m(L)$ to that of pure silicon $\eta_0(L)$ as a function of variation in the lattice constant and symmetric and antisymmetric form factors. The thickness of the silicon film is set at $L = 100$ nm. The range of variation of the lattice constant and the form factors roughly corresponds to that of 0 to 4 at. % doping.

FIG. 3. Imaginary part of the dielectric function of (a) bulk silicon, (b) doped Si_{64} supercells and (c) compensation-doped Si_{128} supercells computed within the DFT/GW-BSE approach of Sec. IV, including the indirect absorption edge as given by Eq. (7). The dashed line in (a) shows the experimental dielectric function from Fig. 1(a). The insets show the indirect absorption region on an expanded scale near 2 eV.

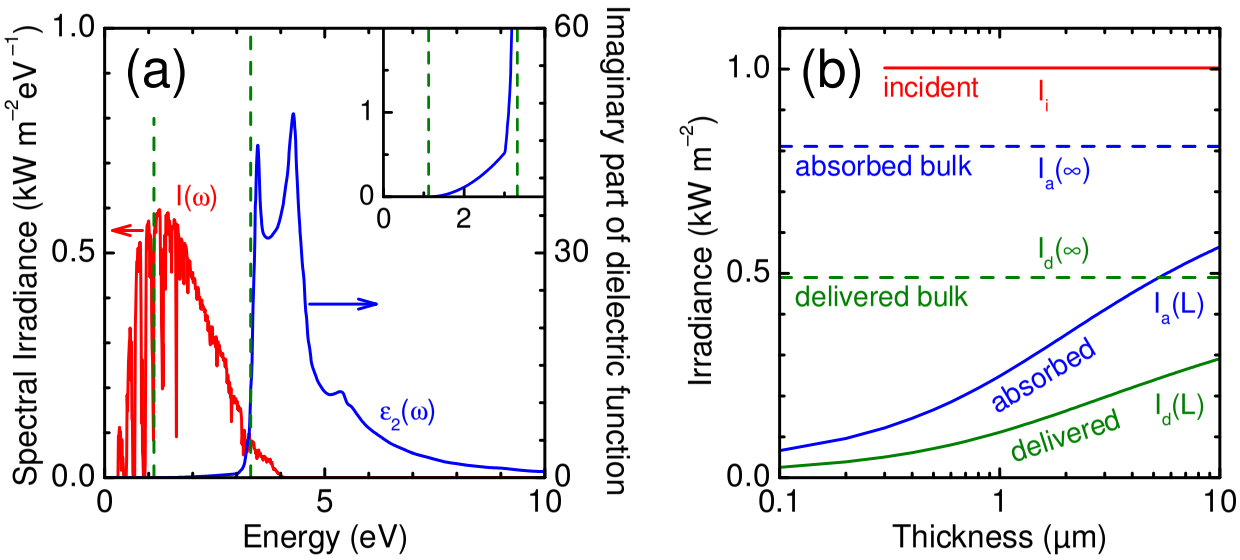

Figure 1 BG12111 14Sep2011

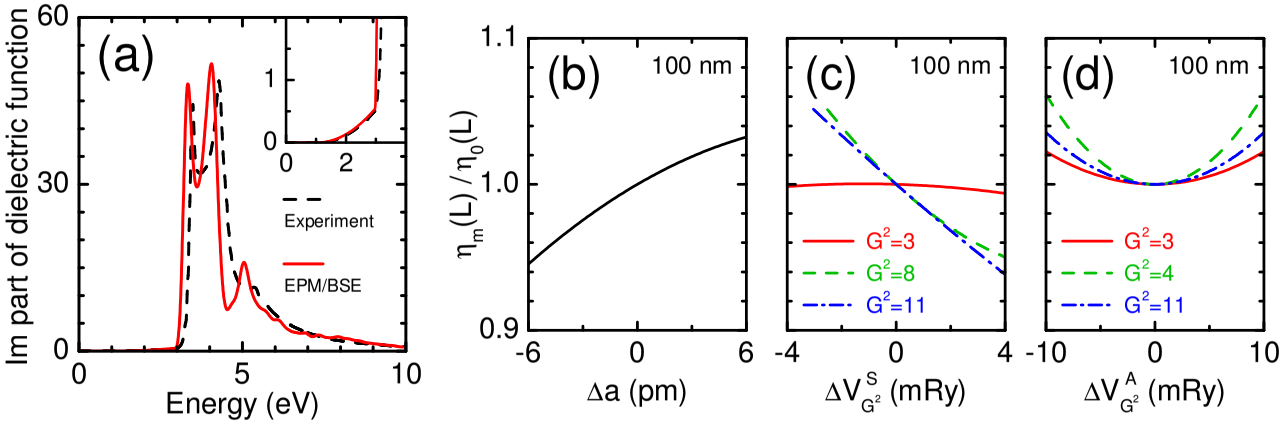

Figure 2 BG12111 14Sep2011

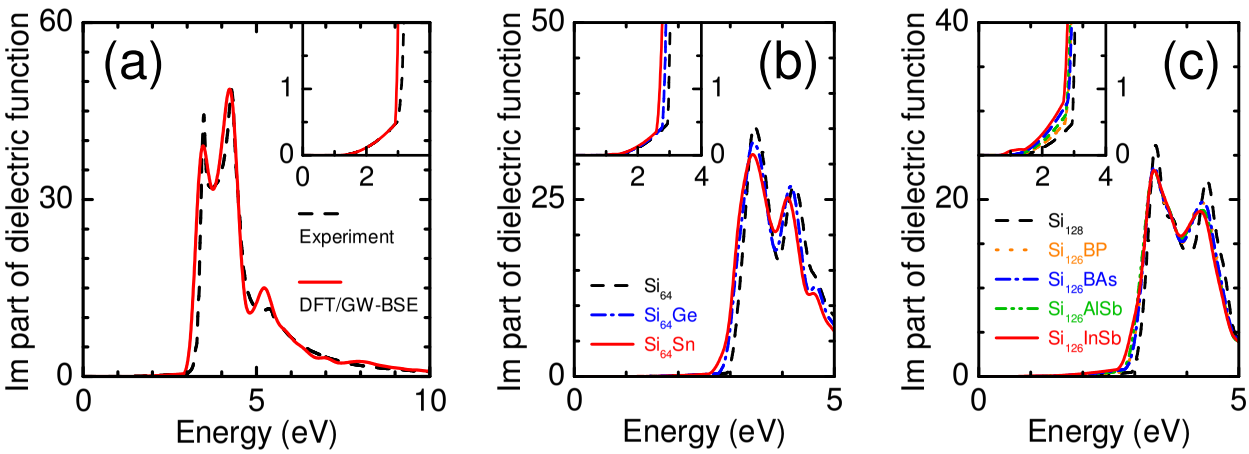

Figure 3 BG12111 14Sep2011